# Perylene–raregas heteroclusters. I. Electronic spectroscopy

Dar Bahatt, Andreas Heidenreich, Narda BenHorin, Uzi Even, and Joshua Jortner

Citation: The Journal of Chemical Physics **100**, 6290 (1994); doi: 10.1063/1.467091
View online: http://dx.doi.org/10.1063/1.467091
View Table of Contents: http://scitation.aip.org/content/aip/journal/jcp/100/9?ver=pdfcov
Published by the AIP Publishing

# Perylene–rare-gas heteroclusters. I. Electronic spectroscopy

Dar Bahatt, Andreas Heidenreich, Narda Ben-Horin, Uzi Even, and Joshua Jortner
*School of Chemistry, Tel Aviv University, Ramat Aviv, 69978 Tel Aviv, Israel*

(Received 30 March 1993; accepted 7 January 1994)

In this paper we report on the electronic two-photon two-color near threshold spectroscopy of mass-resolved perylene·$Ar_n$ ($n=1-45$), perylene·$Kr_n$ ($n=1-35$), perylene·$(N_2)_n$ ($n=1-12$), and perylene·$(CH_4)_n$ ($n=1-10$) heteroclusters. The $S_0\rightarrow S_1$ inhomogeneously broadened spectra of perylene·$Ar_n$ ($n=1-6$) and perylene·$Kr_n$ ($n=1-4$) exhibit resolved spectral features, which were assigned on the basis of experimental combination rules and polarizability relations to the electronic origins of distinct two-sided and one-sided structural isomers. Larger perylene·$A_n$ (A=Ar, Kr; $n=6-10$) heteroclusters exhibit an "abnormal" specific size dependence of the red spectral shifts, which decrease with increasing $n$ and reach a local minimum at $n=8$. Similar characteristics of the red spectral shifts are exhibited for perylene·$(N_2)_n$ and perylene·$(CH_4)_n$ ($n=4-8$) heteroclusters. This abnormal size dependence of the spectral shifts is attributed to the dominance of one-sided single-layered and double-layered structural isomers in this cluster size domain. On the basis of the comparison between the spectroscopic data and molecular dynamics simulations of the absorption line shapes we have obtained a quantitative description of isomer-specific structures for $n=2-6$, a semiquantitative description of the abnormal size domain for $n=6-10$ (due to the dominance of one-sided structures with the abundance of two-layered structures increasing at higher $n$), the prevalence of one-sided structures for $n=16$ and $n=22$, and the realization of two-sided multilayered structures at $n=45$.

## I. INTRODUCTION

Intravalence electronic–vibrational excitations of M·$A_n$ heteroclusters consisting of a large organic aromatic molecule (M) bound to rare-gas atoms or molecular ligands (A)[1-3] are of fundamental interest in relation to the phenomena of specific and universal cluster size effects,[4] microscopic solvation,[1-6] physisorption on microsurfaces,[1(b)] reactive dynamics,[2] isomerization dynamics in large finite systems[3,7,8] and the evolution of condensed matter properties with increasing the cluster size.[4,9] The spectroscopic interrogation of M·$A_n$ heteroclusters by electronic–vibrational spectroscopy provides information on:[1-10] (1) The excited-state energetics as inferred from spectral shifts. (2) The structure and binding of A ligands around the large molecule. (3) The identification of isomers of heteroclusters, which are characterized by isomer-specific spectral properties. (4) Distinct features of surface and interior states of M in and on M·$A_n$ heteroclusters. Such interior and surface states constitute an extreme case of structural isomers. (5) Intermolecular vibrational level structure. (6) Nuclear dynamics of heteroclusters. (7) Homogeneous and inhomogeneous spectral line broadening.

Experimental information on the electronic and electronic–vibrational excited-state energetics[1-26] of these heteroclusters was obtained from the analysis of the absorption spectra of size-selected clusters, interrogated by laser-induced fluorescence,[1,3,5,6] absorption spectroscopy,[23,24] and resonant two-photon–two-color ionization spectroscopy[8,10,22] of a variety of M·$A_n$ clusters [M=tetracene,[8] pentacene,[25] carbazole,[3,11-16,22] benzene,[18-21] naphthalene,[26] 9,10-dichloroanthracene (DCA);[10] A=Ar, Kr, Xe] over a broad size domain. The analysis of the experimental spectral shifts[3,8,10-16,18,21,26] for the components of inhomogeneously broadened absorption bands of size-specific M·$A_n$ clusters established the following characteristics.

(1) Isomer-specific spectral features (for a fixed $n$) were identified, with the isomer structure being established by the application of a microscopic theory of dispersive spectral shifts and by the utilization of empirical combination rules.

(2) Two classes of isomers were spectroscopically identified[3,8-16,18-25] for a fixed $n$: (A) Adcluster isomers ($n'|n-n'$) (Ref. 27) for a fixed $n$ with different structures of the adcluster of $n'$ atoms; (B) structural isomers ($n'|n-n''$) with different occupation numbers $n'$ on the M surface.

(3) The red spectral shifts, $\delta\nu$, for the most abundant isomer of each $n$, reveal a monotonous increase of $|\delta\nu|$ with increasing $n$.

(4) For any M·$A_n$ cluster isomer (of fixed $n$ or $n+1$), $|\delta\nu(\mathrm{M}\cdot\mathrm{A}_n)|<|\delta\nu(\mathrm{M}\cdot\mathrm{A}_{n+1})|$, exhibiting a general monotonous increase of the red spectral shift with increasing the cluster size.

(5) For large clusters an inclination of the saturation of $|\delta\nu|$ with increasing $n$ towards the bulk spectral shift is exhibited, which can be accounted for by a cluster size equation.[4]

Features (1) and (2) are, of course, general. The universality of feature (5) is expected to hold for an interior M in M·$A_n$ clusters. In some heteroclusters, surface M states seem to exist, whereupon the onset of the conversion of $\delta\nu$ to the bulk value is determined by the specific system. Features (3) and (4) were documented in several families of M·$A_n$.[8,10] A notable exception are the carbazole·$Ar_n$ clusters,[12-15] where $|\delta\nu|$ of the apparently inhomogeneous linewidth decreases with increasing $n$ for $n=8-11$ and for $n=13,14$. This inter-

 0021-9606/94/100(9)/6290/10/$6.00 

esting feature was interpreted[12–15] in terms of the formation of double-layered single-sided clusters, i.e., a "wetting–nonwetting transition" for carbazole·$Ar_n$ ($n=8–22$). Another interesting violation of rules (3) and (4) pertains to the isomer-specific shifts of naphthalene·$Ar_n$ ($n=10–15$) clusters,[26] where asymmetric one-layered and two-layered isomers were identified. The violation of rules (3) and (4) is exhibited by the electronic spectra of perylene·$A_n$ (A=Ar, Kr, $N_2$, $CH_4$···) clusters, which is the theme of this paper. We report on the spectroscopy of mass-selected perylene·$Ar_n$ ($n=1–45$), perylene·$Kr_n$ ($n=1–35$), perylene·$(N_2)_n$ ($n=1–12$), as well as perylene·$(CH_4)_n$ ($n=1–10$) heteroclusters. Extensive studies on small perylene·$A_n$ (A=Ar, Kr, $CO_2$, $CH_4$, benzene, hydrocarbons; $n=1–4$) were previously conducted.[28–39] Our work spans a broad size domain of the perylene·$A_n$ clusters, revealing some novel specific spectroscopic size effects. The experimental spectroscopic data for the electronic origin of the $S_0\rightarrow S_1$ transition of small and medium-sized perylene·$Ar_n$ ($n=2–6$) and perylene·$Kr_n$ ($n=2–4$) clusters allow for the resolution of the inhomogeneously broadened absorption band of mass-specific clusters into its isomer-specific components. For $n=1–6$ the size dependence of the spectral shifts of perylene–rare-gas heteroclusters is "normal" obeying features (3) and (4). For larger perylene·$A_n$ (A=Ar, Kr; $n=6–10$) clusters, and for perylene clusters with molecular ligands, i.e., perylene·$A_n$ ($A=N_2$ and $CH_4$; $n=4–8$), a differential blue spectral shift of the inhomogeneous broadened band is exhibited, which is interpreted on the basis of the dominance of one-sided structures of the heteroclusters in this size domain.

## II. $S_0\rightarrow S_1$ EXCITATION SPECTRA OF PERYLENE·$Ar_n$ AND PERYLENE·$Kr_n$ ($n=1–6$)

We have applied the resonant two-photon two-color ionization (R2P2CI) method to interrogate the $S_0\rightarrow S_1$ excitation spectra of perylene with Ar, Kr, $N_2$, and $CH_4$. Measuring the excitation spectrum with the energy of the ionizing laser just above threshold, we were able to obtain the spectra with minimum excess energy ($<100$ cm$^{-1}$) above ionization and to avoid fragmentation. Our experimental techniques for the supersonic nozzles, for the production of cluster beams, R2P2CI, and mass-spectrometric detection were previously described.

The R2P2CI spectrum for the $S_0\rightarrow S_1$ original vibrational excitations of the jet cooled bare perylene molecule is in good agreement with previous laser induced fluorescence spectra[28,40] and absorption spectra.[41] The R2P2CI spectrum reveals the electronic origin of the $S_0\rightarrow S_1$ transition at 4155.2 Å followed by low 96 and 167 cm$^{-1}$ vibrational features, which correspond to $2v$ vibrational overtones of the "ungerade butterfly" mode and "gerade accordion" mode of intramolecular vibrations.[40,42] Representative mass-resolved R2P2CI $S_0\rightarrow S_1$ spectra of perylene·$Ar_n$ ($n=1–45$) and perylene·$(N_2)_n$ ($n=1–12$) in the vicinity of the electronic origin are displayed in Figs. 1 and 2. Small and medium-sized perylene·$Ar_n$ ($n=1–7$) and perylene·$Kr_n$ ($n=1–5$) heteroclusters (Fig. 1) exhibit resolved spectral features, which are amenable to a conventional spectroscopic analysis. The analysis of the spectral features for perylene·$Ar_n$ ($n=1–6$) and perylene·$Kr_n$ ($n=1–4$) heteroclusters (Tables I and II) rests on: (i) The assignment of the most intense features to the electronic origins of structural isomers (labeled as I, II, III). (ii) The intramolecular vibrational excitations of isomers. The frequency of the perpendicular $z$ vibration for perylene·$Ar_n$ ($n=1–6$) was $\nu_z=43–47$ cm$^{-1}$, while $\nu_z=36–38$ cm$^{-1}$ for perylene·$Kr_n$ ($n=1–3$). These vibrations are exhibited for several perylene·$A_n$ isomers. The vibrational frequencies of the $z$ vibration of perylene·$A_n$ (A=Ar, Kr) are similar to those of other M·$A_n$ heteroclusters. The relative intensities of the $z$ vibration of small perylene·$Ar_n$ and perylene·$Kr_n$ are high ($I\simeq 0.3–0.5$), being higher than those for DCA·$Ar_n$ (Ref. 10) and tetracene·$Ar_n$.[8] (iii) The intramolecular $\nu_i=96$ cm$^{-1}$ vibration[28,40,42] is clearly exhibited for perylene·$A_n$ (A=Ar, Kr; $n=1–3$) and possibly also for $n=4$ clusters. Clustering of perylene does not grossly modify the low-frequency butterfly overtone vibration, although broadening of these spectral features is exhibited. A similar trend was observed for the low-frequency overtone vibration of pentacene. The results of our analysis (Tables I and II) confirm and extend Leutwyler's LIF results for $n=1–3$. Structures of isomers for perylene·$Ar_n$ ($n=1–6$) and perylene·$Kr_n$ ($n=1–4$) were assigned on the basis of experimental combination rules,[10] with the spectral shift $\delta\nu(n|m)$ for the $(n|m)$ structure being expressed as the sum of contributions from the one-sided $(n|0)$ and $(0|m)$ substructures, i.e., $\delta\nu(n|m)=\delta\nu(n|0)+\delta\nu(0|m)$. This relation allowed for the identification of structures for perylene·$Ar_n$ ($n=1–6$), presented in Table III and perylene·$Kr_n$ ($n=1–4$), presented in Table II. While for small clusters $n=2$ and 3 the most abundant clusters involve the two-sided structures, one-sided structures were observed for perylene·$Ar_n$ ($n=1–6$). In contrast to other M·$A_n$ (M=tetracene, DCA; A=Ar, Kr, Xe) heteroclusters, where the one-sided structures were identified only for smaller ($n\leq 4$) clusters, the one-sided structures, involving "surface states" of perylene·$Ar_n$, are ubiquitous for larger clusters, being identified on the basis of the combination rules up to $n=6$ (Table III). The relative intensities of the "surface states" are large (Table I), so that their relative abundance is close to that of the two-sided isomers.

An independent experimental assignment of the isomer-specific spectral shifts for perylene·$A_n$ (A=Ar, Kr; $n=1–4$) heteroclusters rests on the dependence of $\delta\nu(n|m)$ on the atomic polarizability $\alpha$ of the rare-gas atom. The microscopic theory of dispersive spectral shifts predicts that[6,43] $\delta\nu(n|m)=\alpha B(n|m)$, where $B(n|m)$ is a product of an electronic and a geometrical factor. $B(n|m)$ is isomer-specific, but is expected to exhibit only a weak dependence on the nature of the rare-gas atom, slightly decreasing with the increase of the atomic radius of A.[43] Accordingly, one expects that for an isomer-specific cluster $\delta\nu(n|m)\propto\alpha$. This polarizability relation of $\delta\nu$ was established since the early studies of M·$A_n$ cluster spectra for the smallest M·$A_1$ (A=Ar, Kr, Xe) clusters where $\delta\nu(1|0)\propto\alpha$.[1,6] In Fig. 3 we demonstrate the polarizability relation for the isomer-specific spectral shifts of perylene·$Ar_n$ and perylene·$Kr_n$ ($n=1–4$). The spectral shifts for the Ar and Kr isomer-specific clusters are linearly related by $\delta\nu$(perylene·$Kr_n$)$=\beta\delta\nu$(perylene·$Ar_n$) with $\beta=1.42$. This experimental value of $\beta$ is close to the ratio of

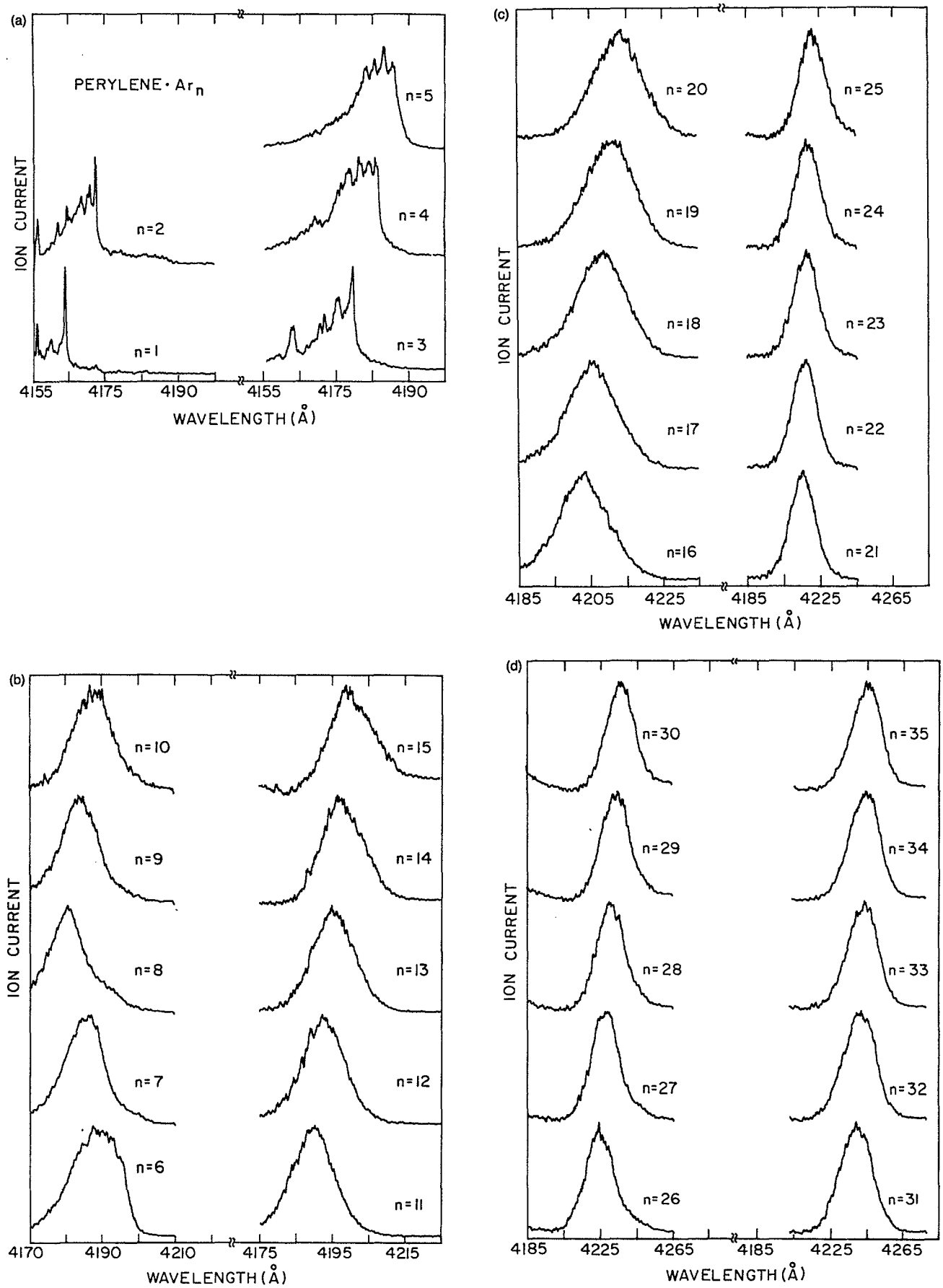


FIG. 1. R2P2CI mass-resolved $S_0 \rightarrow S_1$ spectra of perylene·$Ar_n$ ($n=1-45$). The expansion mixture contained 10%Ar and 90%Ne70 (70%Ne+30%He). The stagnation pressures were 1–3 atm. Nozzle temperature 200 °C. (a): $n=1-5$. (b): $n=6-15$. (c): $n=16-25$. (d): $n=26-35$. (e): $n=36-45$.

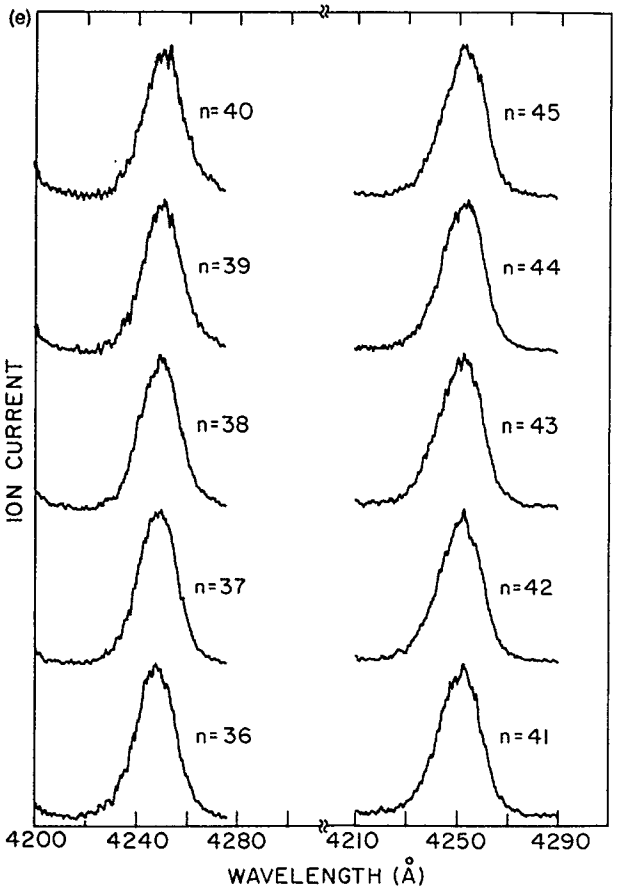


FIG. 1. (*Continued.*)

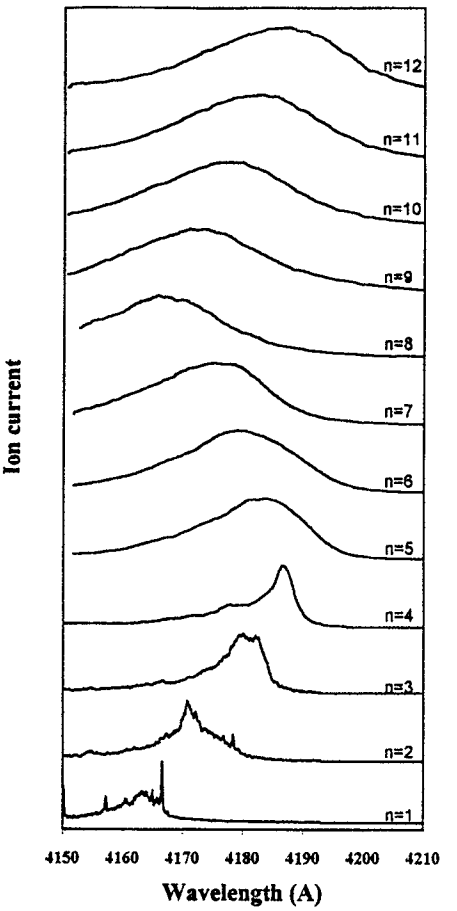


FIG. 2. R2P2CI spectra of perylene·$(N_2)_n$ ($n=1-12$). The expansion mixture contained 10%$N_2$ and 90%Ne70. Experimental conditions as in Fig. 1.

the polarizabilities $\alpha(\mathrm{Kr})/\alpha(\mathrm{Ar})=1.50$ of the Kr and Ar atoms, with the slight deviation of $\beta$ from the polarizability ratio being due to the weak dependence of $B(n|m)$ on the nature of the rare-gas atoms. The experimental assignment of the isomer structures on the basis of combination rules and polarizability relations is further supported by the MD simulations of the spectral lineshapes, which will be reported in the subsequent paper.[44] The spectral shifts obtained from the simulations of the line shapes (Table III) provide theoretical information on isomer-specific spectral shifts. The good agreement accomplished between experiment and simulations[44] (Table III) provides independent evidence for the assignment of the isomer-specific spectral features.

## III. TRENDS IN SPECTRAL SHIFTS AND LINEWIDTHS OF PERYLENE–RARE-GAS CLUSTERS

Figures 4 and 5 present the size dependence of the red spectral shifts ($\delta\nu<0$) for perylene·$Ar_n$ ($n=1-45$) and perylene·$Kr_n$ ($n=1-35$) heteroclusters. The spectral shifts exhibit three regions: (i) Small and medium-sized clusters with $n=1-6$. Isomer specific spectral shifts (for a given $n$), which were already discussed, are exhibited. The red spectral shifts increase with increasing $n$, i.e., the differential spectral shift $D\nu(n)=[\delta\nu(n)-\delta\nu(n-1)]$ is negative, $[D\nu(n)<0]$ for $n=2-6$. (ii) The abnormal region for $n=6-10$. For perylene·$Ar_n$ ($n=6,7$), a spectral structure, which is attributed to structural isomers, is still observed and is included in Fig. 4, while for perylene·$Ar_n$ ($n=8-10$) and perylene·$Kr_n$ ($n=6-10$) the peak of the broad structureless spectral feature was taken for the estimate of the spectral shift. In this size domain the red spectral shifts for both Ar and Kr heteroclusters exhibit a decrease of $|\delta\nu|$ with increasing $n$ for $n=6-8$. A local minimum of $|\delta\nu|$ is exhibited at $n=8$ for both Ar and Kr clusters and then $|\delta\nu|$ starts increasing with increasing $n$ for $n=8-10$. The differential blue shift $[D\nu(n)>0]$ for $n=6-8$ is unique for these perylene clusters, violating the general trends of the monotonous sublinear increase of $|\delta\nu|$ with increasing $n$, i.e., differential red spectral shifts, for other M·$A_n$ heteroclusters.[8,10] This unique specific cluster size dependence will be explored in Secs. IV and V. (iii) Large clusters. For $n>10$, the red spectral shift $|\delta\nu|$ (determined at the peak of the broad spectral feature) reveals a sublinear increase with increasing $n$. For perylene·$Ar_n$ at $n\simeq25$, an onset of a further increase of the differential red spectral shift $[D\nu(n)<0]$ with increasing $n$ is exhibited, and a similar, though less pronounced, feature is exhibited also for perylene·$Kr_n$ at $n\simeq20$. For larger heteroclusters ($n>30$), an inclination of the saturation of $\delta\nu$ with increasing $n$ is revealed, reaching the value of $\delta\nu=-568$ $\mathrm{cm}^{-1}$ for perylene·$Ar_{45}$.

The size dependence of the experimental spectral lin-

TABLE I. Spectral features of mass-resolved perylene·$Ar_n$ ($n=1-7$) clusters.

| $n$ | Cluster energy $-\delta\nu$ ($cm^{-1}$)[a] | Cluster energy $\Delta\nu_0''$($cm^{-1}$)[b] | Relative intensity[c] | Assignment Isomer vibrations[d] | | Tentative identification of isomers[e,f] |
|---|---|---|---|---|---|---|
| 1 | 51.5 | 0 | 1.0 | I | 0 | I(1\|0) |
| | 31 | 22 | 0.2 | | | |
| | 5 | 47 | 0.3 | I | $z$ | |
| | 44 | 96 | 0.4 | I | $i$ | |
| 2 | 102 | 0 | 1.0 | I | 0 | I(1\|1) |
| | 94 | 8 | 0.7 | II | 0 | II(2\|0) |
| | 80 | 22 | 0.5 | | | |
| | 56 | 46 | 0.5 | I | $z$ | |
| | 50 | 52 | 0.4 | II | $z$ | |
| | 6 | 96 | 0.5 | I | $i$ | |
| 3 | 142 | 0 | 1.0 | I | 0 | I(2\|1) |
| | 120 | 22 | 0.6 | II | 0 | II(3\|0) |
| | 96 | 46 | 0.5 | I | $z$ | |
| | 90 | 52 | 0.4 | | | |
| | 48 | 94 | 0.4 | I | $i$ | |
| 4 | 178 | 0 | 1.0 | I | 0 | I(2\|2) |
| | 167 | 11 | 0.9 | II | 0 | II(3\|1) |
| | 151 | 27 | 1.0 | III | 0 | III(4\|0) |
| | 135 | 43 | 0.9 | I | $z$(?) | |
| | 124 | 54 | 0.7 | II | $z$(?) | |
| 5 | 207 | 0 | 0.9 | I | 0 | I(3\|2) |
| | 192 | 15 | 1.0 | II | 0 | II(4\|1) |
| | 178 | 29 | 0.9 | ? | | |
| | 164 | 43 | 0.8 | III | 0 | III(5\|0) |
| 6 | 238 | 0 | 0.7 | I, II | | I(3\|3) |
| | 218 | 20 | 0.9 | III | | II(4\|2) |
| | 203 | 35 | 0.9 | ? | | III(5\|1) |
| | 189 | 49 | 0.9 | IV | | IV(6\|0) |
| 7 | 195 | 0 | 0.9 | I | | I(7\|0) |
| | 182 | 13 | 1.0 | ? | | |
| | 169 | 28 | 0.9 | ? | | |

[a]Energetic shift from the $S_1$ electronic origin of the bare molecule.
[b]Energetic shift from the lowest energy spectral feature of the heterocluster of a given composition.
[c]The intensity of the most prominent spectral feature is taken as 1.0.
[d]The intermolecular vibration is labeled as $z$ perpendicular, and the intramolecular butterfly vibration is labeled as $i$.
[e]Electronic origins of structural isomers are labeled as I,II,III..., .
[f]Structures of heteroclusters are labeled as ($n|m$), marking $n$ atoms on one side and $m$ atoms on the other side of the aromatic molecule, both $n$ and $m$ being in the first layer.

ewidths is also presented in Figs. 4 and 5. For small $n=1-3$ heteroclusters the spectral features, which correspond to distinct structural isomers (at fixed $n$), can be well separated and we present the linewidth, i.e., the full width at half maximum (FWHM) of the electronic origin of the prominent isomer. These linewidths for small ($n=1-3$) clusters, which correspond to (presumably homogeneous and inhomogeneous) broadening of a single isomer, with the linewidth increasing with increasing $n$. For larger ($n=4-7$) heteroclusters, the spectral overlap between distinct isomer-specific features is extensive, whereupon it is difficult to extract the individual isomer-specific linewidths. For these ($n=4-7$) and for large ($n>7$) heteroclusters, we present (Figs. 4 and 5) the FWHM of the entire spectral distribution for each group of heteroclusters of a given value of $n$. The spectral widths for $n>4$ manifest the inhomogeneous line broadening due to the coexistence of spectrally overlapping structural isomers, with the spectral features, i.e., the electronic origin and the intermolecular vibrations of each distinct isomer, being (presumably) homogeneously broadened. The pronounced jump of the linewidths between $n=3$ and $n=4$ (Figs. 4 and 5) reflects the difference between single isomer homogeneous and inhomogeneous line broadening and (spectrally congested) inhomogeneous broadening due to the existence of several isomers. The inhomogeneous linewidth reflects a weak size dependence in the broad size domain $n=4-45$, e.g., for perylene·$Ar_n$ the inhomogeneous linewidth increases by ~20% in the range $n=4-45$. Some specific size effects (~10%–20%) on the inhomogeneous linewidth cannot be excluded.

## IV. THE ABNORMAL SIZE DOMAIN FOR SPECTRAL SHIFTS

The observation of the decrease of $|\delta\nu|$ with increasing $n$ [i.e., $D\nu(n)>0$] in the size domain $n=6-8$ with a local minimum of $|\delta\nu|$ at $n=8$ for perylene·$Ar_n$ and perylene·$Kr_n$ clusters appears to be a general feature for perylene·$A_n$ het-

TABLE II. Spectral features of mass-resolved perylene·$Kr_n$ ($n=1-4$) clusters.[a]

| | Cluster energy | | Tentative assignment | | $-\delta\nu$ ($cm^{-1}$) Estimated from combination rules |
|---|---|---|---|---|---|
| $n$ | $-\delta\nu$ ($cm^{-1}$) | $\Delta_0^{\nu}$ ($cm^{-1}$) | Isomer vibration | | |
| 1 | 76 | 0 | I(1\|0) | | |
| | 38 | 38 | I(1\|0) | $z$ | |
| | −18 | 94 | I(1\|0) | $i$ | |
| 2 | 148 | 0 | I(1\|1) | | 152 |
| | 129 | 19 | II(2\|0) | | |
| | 125 | 23 | | | |
| | 112 | 36 | I(1\|1) | $z$ | |
| | 104 | 44 | | | |
| | 90 | 58 | II(2\|0) | $z$ | |
| | 86 | 62 | | | |
| | 54 | 94 | I(1\|1) | $i$ | |
| | 31 | 117 | II(2\|0) | $i$ | |
| 3 | 202 | 0 | I(2\|1) | | 205 |
| | 166 | 36 | I(2\|1) | $z$ | |
| | 155 | 47 | II(3\|0) | | |
| | 151 | 51 | | | |
| | 105 | 97 | I(2\|1) | $i$ | |
| 4 | 251 | 0 | I(2\|2) | | 258 |
| | 238 | 13 | II(3\|1) | | 231 |
| | 223 | 28 | II(4\|0) | | |
| | 205 | 46 | | | |

[a]Notation as in Table I.

eroclusters, since similar characteristics are exhibited for the spectral shifts of perylene heteroclusters with molecular ligands, i.e., perylene·$(N_2)_n$ and perylene·$(CH_4)_n$. In the spectra of these heteroclusters, $\delta\nu$ (for $n>2$) was again determined from the peak of the broad inhomogeneously broadened spectral feature in the R2P2CI $S_0\rightarrow S_1$ spectra. A cursory examination of the spectra of perylene·$(N_2)_n$ ($n=1-12$) clusters (Fig. 2) clearly reveals the decrease of $|\delta\nu|$ with increasing $n$ in the range $n=4-8$, with a local minimum of $|\delta\nu|$ at $n=8$. In Fig. 6 we summarize the size dependence of the spectral shifts of perylene·$(N_2)_n$ and perylene·$(CH_4)_n$ clusters together with the spectral shifts of the Ar and Kr heteroclusters, which are included for the sake of comparison. The spectral shifts of the molecular ligands reveal blue differential shifts at $n=4-8$ for perylene·$(N_2)_n$ and a nearly

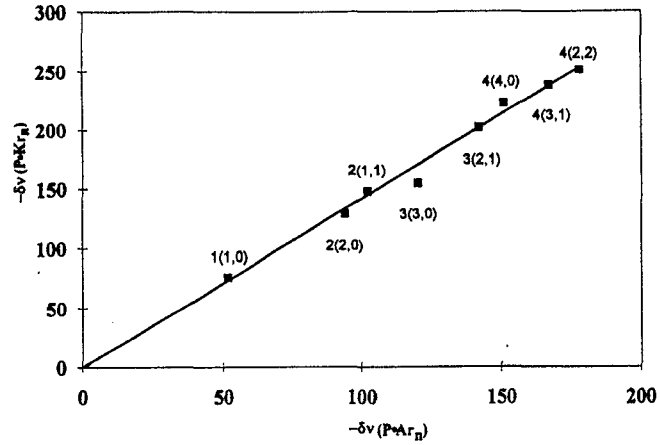


FIG. 3. Isomer-specific spectral shifts of perylene (P) clusters with Ar and Kr. The P·$Ar_n$ and P·$Kr_n$ clusters are labeled as $(n|n-m)$. The spectral shifts for the Ar and Kr isomer-specific clusters are related by $\delta\nu(P\cdot Kr_n)=\beta\delta\nu(P\cdot Ar_n)$ with $\beta=1.42$.

TABLE III. Electronic origin of perylene·$Ar_n$ ($n=1-7$) clusters.

| $n$ | Isomer[a] | $-\delta\nu$ ($cm^{-1}$) Experimental[a] | $-\delta\nu$ ($cm^{-1}$) Calculated[b] | $-\delta\nu$ ($cm^{-1}$) Estimated from combination rules[c] |
|---|---|---|---|---|
| 1 | (1\|0) | 51.5 | 54 | |
| 2 | (1\|1) | 102 | 106 | 103 |
| | (2\|0) | 94 | 91 | |
| 3 | (2\|1) | 142 | 142 | 145 |
| | (3\|0) | 120 | 123 | |
| 4 | (2\|2) | 178 | 182 | 188 |
| | (3\|1) | 167 | 177 | 172 |
| | (4\|0) | 151 | 146 | |
| 5 | (3\|2) | 207 | 213 | 214 |
| | (4\|1) | 192 | 199 | 203 |
| | (5\|0) | 164 | 165 | |
| 6 | (3\|3) | 238 | 246 | 240 |
| | (4\|2) | | 236 | 245 |
| | (5\|1) | 218 | 218 | 216 |
| | (6\|0) | 189 | 186 | |
| 7 | (7\|0) | 195 | 209 | |
| | (6\|1) | | 240 | 241 |
| | (5\|2) | | 256 | 258 |
| | (4\|3) | | 270 | 271 |

[a]Experimental spectral shifts and assignments of electronic origins of isomers from Fig. 2 and Table I.

[b]Calculated spectral shifts using excited-state potential parameters LJ2 (Ref. 44).

[c]Combination rule for spectral shifts of origins: $\delta\nu(n|m)=\delta\nu(n|0)+\delta\nu(0|m)$.

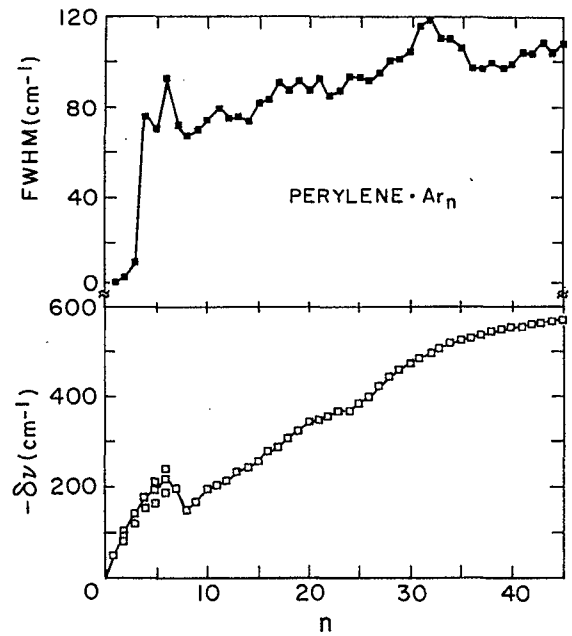


FIG. 4. The size dependence of the spectral shifts ($\delta\nu$) and linewidths (FWHM) of perylene·$Ar_n$ heteroclusters. Lower part: spectral shifts of the distinct structural isomers for $n=1-6$ and the mean spectral shifts for $n=7-45$. Upper part: Width of the single (lowest energy) isomer for $n=1-3$ and for the total spectral distribution for $n=4-45$.

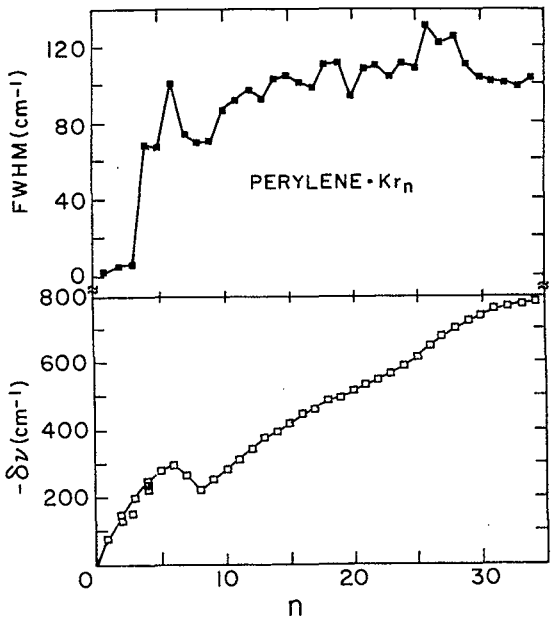


FIG. 5. The size dependence of the spectral shifts ($\delta\nu$) and linewidths (FWHM) of perylene·$Kr_n$ heteroclusters. Lower part: isomer specific spectral shifts for $n=1-4$ and mean spectral shifts $n=5-34$. Upper part: Widths of the single lowest energy isomer for $n=1-3$ and of the total spectral distribution for $n=4-34$.

constant value of $\delta\nu$ for $n=4-8$ for perylene·$(CH_4)_n$. For both perylene·$(N_2)_n$ and perylene·$(CH_4)_n$, a minimum of $|\delta\nu|$ at $n=8$ is exhibited. It is interesting to note that the spectral shift for the perylene·$(N_2)_8$ cluster is close to $\delta\nu$ for perylene·$(N_2)$ (Fig. 6), although, of course, inhomogeneous broadening in the case of perylene·$(N_2)_8$ is excessive, while perylene·$N_2$ exhibits a sharp electronic origin (Fig. 2). From Fig. 6 it is apparent that the perylene heteroclusters with both molecular ligands and with rare-gas atoms exhibit a similar abnormal behavior of the spectral shifts of the inhomogeneously broadened bands. As the most detailed spectroscopic information is available for perylene–rare gas heteroclusters, we shall restrict our discussion to these systems. Two classes

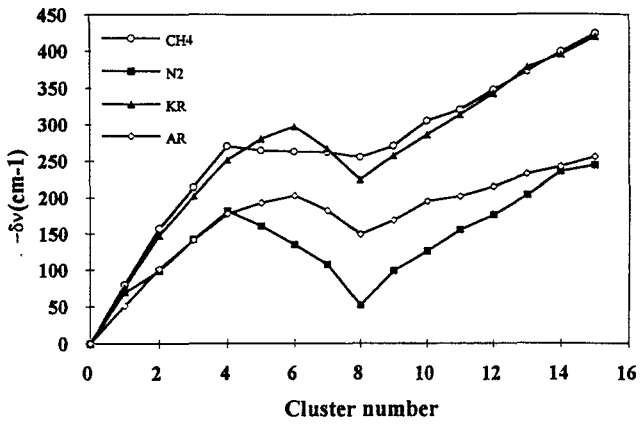


FIG. 6. The size dependence of the mean spectral shifts of perylene·$A_n$ (A=Ar, Kr, $N_2$, $CH_4$) heteroclusters.

of dynamic and structural phenomena should be considered in an attempt to explain the abnormal spectral shifts.

(A) Dynamic effects of isomerization. Previous work[7,8] on MD and Monte Carlo simulations established a hierarchy of heterocluster isomerization processes with increasing temperature, i.e., (i) restricted correlated surface motion, (ii) correlated surface motion, (iii) uncorrelated surface motion (surface melting), (iv) 2D⇄3D wetting–nonwetting, and (v) side crossing. Simulations of spectroscopic observables (spectral shifts and central second moments) for DCA·$Ar_n$ and tetracene·$Ar_n$ clusters revealed that the temperature and size dependence of $\delta\nu$ are rather insensitive to isomerization processes (i)–(iv), while process (v) exhibits a marked effect on the central second spectral moment. Side crossing isomerization takes place at relatively high temperatures ($T>40$ K), which exceed typical experimental M·$A_n$ heterocluster temperatures.[8,10,26,45] Accordingly, the dynamic effects of isomerization, giving rise to the abnormal spectral shifts, can be precluded.

(B) Abundance of one-sided structural isomers. The spectroscopic analysis of isomer-specific $\delta\nu$ for perylene·$Ar_n$ ($n\leq 6$) clusters established the coexistence of two-sided and one-sided isomers, e.g., for $n=6$ we identified the (3|3), (4|2), (5|1), and (6|0) isomers (Tables I and III). The one-sided ($n|0$) structure is characterized by the lowest value of $|\delta\nu|$ for all isomers of a fixed $n$, as it is also the case for other M·$A_n$ (M=DCA, tetracene, naphthalene) heteroclusters, being in accord with the microscopic theory of dispersive spectral shifts. For perylene·$Ar_n$ clusters, the one-sided structures ($n|0$) are abundant for low and moderate $n$ ($\leq 6$). The abnormal spectral shifts for $n=6-10$ heteroclusters can arise from the abundance of one-sided ($n|0$) structural isomers in this size domain.

We attribute the decrease of $|\delta\nu|$ with increasing $n$ (for $n=6-8$) to the dominance of one-sided ($n|0$) isomers, which correspond to "surface states" of these heteroclusters. There are some precedents for this physical picture. The existence of one-sided isomers of carbazole·$Ar_n$ ($n=8-14$) was invoked by Leutwyler *et al.*,[12,13] one-sided small benzene·$Ar_n$ ($n=2-6$) heteroclusters were assigned by Schmidt *et al.*[20] on the basis of $S_0\rightarrow S_1$ spectroscopy and ionization potential data, the dominance of benzene surface states for large benzene·$Ar_n$ ($n=25$) clusters was proposed by Whetten *et al.*[46] on the basis of the nonconvergence spectral shifts to their bulk value, and the existence of a benzene·$Ar_{19}$ surface state was proposed by Adams and Stratt[47] on the basis of MD simulations. For perylene·$Ar_n$ ($n=6-8$) and other perylene heteroclusters in this size domain, we propose that the differential blue spectral shifts (determined for the dominant spectral features of $n=6-8$) originate from the abundance of $n=7$ and 8 one-sided structures. The experimental line broadening of the $n=7$ and $n=8$ isomers originates from the coexistence of one-sided structures, e.g., one-sided single-layered ($0|n$), and two-layered ($0|m+m_2$) with $m+m_2=n$. The spectral shifts of the ($0|n$) and ($0|m+m_2$) isomers are expected to differ with $|\delta\nu(0|n)|>|\delta\nu(0|m+m_2)|$, giving rise to inhomogeneous broadening due to coexistence of distinct isomers. At higher (yet unknown) temperatures 2D⇄3D isomerization processes between one-sided isomers

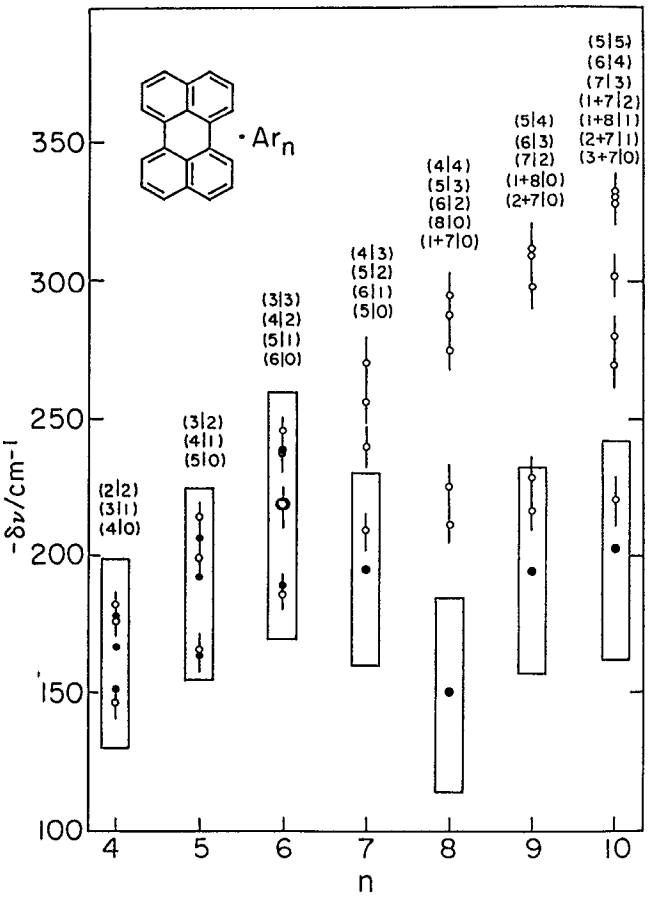


FIG. 7. An analysis of the abnormal region of the spectral shifts based on the comparison between the simulated spectral shifts (Ref. 44) for two-sided and one-sided isomers and the experimental data for perylene·$Ar_n$ ($n=4$–10). The simulated (LJ2 potential parameters at $T=30$ K) isomer specific spectral shifts from the subsequent paper (Ref. 44) (○) are labeled by the isomer structures, which are marked in order of decreasing $|\delta\nu|$ for each $n$. The error bars represent the linewidths $\Gamma$. The experimental spectral shifts (●) represent the peak energies of the isomers for $n=4$–6 and of the structureless spectral distribution for $n=7$–10. The long axes of the "boxes" represent the experimental linewidths (FWHM) of the distribution of the total spectral feature(s) for each $n$.

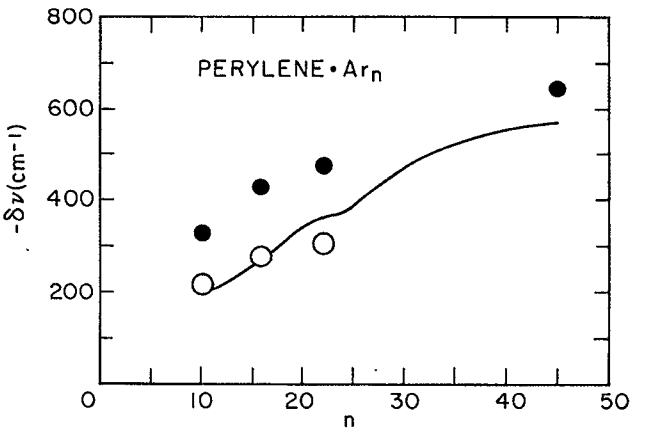


FIG. 8. Analysis of the spectral shifts for large perylene·$Ar_n$ ($n=10$–45) clusters. The solid line represents the experimental spectral shifts of the structureless spectral features. The calculated spectral shifts at 30 K from the subsequent paper (Ref. 44) correspond to the following one-sided structures (○): $n=10(3+7|0)$, $n=16$ (averaged one-sided structure with 2D⇄3D isomerization), $n=22$ (averaged one-sided triple layered structure) and to the following two-sided structures (●): $n=10(5|5)$, $n=16$ [averaged two-sided containing 40% of (8|8) and 37% of (9|7)], $n=22$ [averaged two-sided containing dominant contributions of (14|8), (15|17), (14|7)+1$s$, (138)+1$s$] and $n=45$ (averaged two-sided structure containing 40 two-sided structural isomers $(n_2+n'|m_2+m'+n_s$ with $n_s=0$–8 and $n_2+n'=20$–30).

will occur and the nuclear isomerization dynamics will contribute to the spectral line broadening. On the basis of the analogous (but different) tetracene·$Ar_n$ clusters we can roughly infer that such one-sided isomerization processes for $n>6$ will set in at $T\gtrsim 30$ K. At even higher temperatures ($T\gtrsim 45$ K) side crossing isomerization between one-sided and two-sided isomers are expected to set in.[44] It appears that our experimental conditions pertain to lower temperatures, whereupon the one-sided clusters will preserve their identity.

## V. CONFRONTATION BETWEEN SPECTROSCOPIC OBSERVABLES AND SIMULATED ABSORPTION LINE SHAPES

We now proceed to the identification of the structural isomers on the basis of molecular dynamics simulations of the absorption line shapes and, in particular, the spectral shifts, which are reported in the subsequent paper.[44] This analysis will provide theoretical evidence for the dominating contribution of the one-sided $(n|0)$ isomers in the abnormal size domain ($n=6$–10) and provide an overall physical picture for the size-dependent "transition" between surface-type states and interior states of perylene on and in Ar clusters for perylene·$Ar_n$ ($n=10$–45) clusters.

In Fig. 7 we present a comparison between the experimental spectral shifts for $n=4$–10 clusters with the simulated $\delta\nu$ data at 30 K, calculated in the subsequent paper[44] with the LJ2 potential parameters (presented in Ref. 44). In Fig. 7 we also included the experimental inhomogeneous total linewidths of the entire distribution of isomers and the simulated linewidths $\Gamma$ (at 30 K) of the total line shapes.[44] For $n=4$–6 good agreement is achieved between the simulated spectral shifts for the entire distribution of the structural isomers $(n/2|n/2)$, $(n/2+1|n/2-1)\cdots(n|0)$ and the experimental spectral shifts. The inhomogeneous (total) spectral linewidths of the individual isomer-specific absorption bands for $n=4$–6 spans the experimental total inhomogeneous linewidth. On the other hand, the simulations show that for $n=7$–10 the two-sided isomers are characterized by large red spectral shifts, which are considerably higher than the experimentally observed spectral shift range (Fig. 7). Thus two-sided structures are practically excluded in this size domain. The upper part of the experimental range of the red spectral shifts for $n=7$ is consistent with the simulated (7|0) one-sided isomer, the upper part of the experimental $\delta\nu$ for $n=8$–10 is compatible with one-sided one-layered $(n|0)$ and two-layered $(m_2+7|0)$ structures. The physical picture emerging from the present analysis indicates the dominance of one-sided structural isomers for $n\geq 6$ with the abundance of one-sided two-layered structures increasing with increasing $n$.

For large ($n>10$) perylene·$Ar_n$ clusters the red spectral

shift rises monotonously with increasing $n$ (Fig. 4). One should inquire what the dominating heterocluster structures in the large size domain are, as inferred from the spectral shifts. In the subsequent paper[44] we report on the simulated absorption line shapes at 30 K for two-sided and for one-sided $n=16$ and $n=22$ clusters and for the two-sided $n=45$ cluster. For perylene$\cdot Ar_{16}$ the simulated red spectral shifts for the two-sided isomer mixture and for the individual two-sided isomers are considerably larger than the experimental spectral shift (Fig. 8), so that two-sided $n=16$ structures can be excluded. The spectral shift for the one-sided single-layered $(16|0)$ structure is in good agreement with the experimental $\delta\nu$ (Fig. 8). For perylene$\cdot Ar_{22}$ the simulated[44] inhomogeneous red spectral shift for the two-sided structures again considerably exceeds the experimental value (Fig. 8). The experimental spectral shift for perylene$\cdot Ar_{22}$ can be accounted for in terms of a superposition of one-sided structures $(22|0)$ and one-sided structures with peripheral atoms, e.g., $(22-m_s|0)+m_s$ (with small $m_s$).[27] The large experimental linewidths ($\Gamma_{expt}=84$ cm$^{-1}$ for $n=16$ and $\Gamma_{expt}=85$ cm$^{-1}$ for $n=22$) are consistent with an inhomogeneous composite line broadening. We thus conclude that large perylene$\cdot Ar_n$ ($n=16-22$) clusters are dominated by one-sided structures, with the contribution of one-sided structures with peripheral atoms increasing at $n\simeq 22$.

The foregoing analysis provides a rather unique physical picture for perylene$\cdot Ar_n$ heteroclusters in the size domain $6<n\lesssim 22$, with the prevalence of surface-type states, i.e., the perylene microsurface supporting a single-layer or a "droplet" of Ar atoms. An interesting question in the general context of cluster size effects is: At what heterocluster size will an interior state of perylene in Ar heteroclusters be realized? For perylene$\cdot Ar_{45}$ the simulated red spectral shift for the two-sided structure[44] is only somewhat higher (by 15%) than the experimental value (Fig. 8), indicating that for $n=45$ the two-sided multilayered structure dominates. The large simulated total linewidth for this two-sided structure[44] ($\Gamma=85$ cm$^{-1}$ at 30 K) is in reasonable agreement with the experimental value $\Gamma_{expt}=104$ cm$^{-1}$. This physical picture for the realization of an internal state of perylene in $Ar_n$ ($n=45$) clusters will imply that the experimental onset of a further increase of $\delta\nu$ with increasing $n$ for $n>25$ (Fig. 4) marks the "transition" from one-sided multilayer structures to two-sided internal structures.

## VI. CONCLUDING REMARKS

The excited-state energetics, which is expressed in terms of the spectral shifts, provides a tool for the identification of distinct, noninterconverting configurations of $M\cdot A_n$. The spectral shifts represent the cumulative energetic contributions of the M–A interactions. The multimodal distribution of the spectral shifts of distinct structural isomers provides a powerful tool for the identification of isomer-specific structures. An extreme case of structural isomer specificity pertains to the distinction between surface and interior states of M on or in the $M\cdot A_n$ heteroclusters, which are pertinent for the spectroscopy of perylene$\cdot Ar_n$.

From the experimental point of view the present analysis requires several extensions. First, the cluster temperature cannot yet be experimentally determined. The simulation data used for this analysis were taken at 30 K. We shall address elsewhere[48] the interesting issue of the temperature dependence of the spectral line shapes, of $\delta\nu$, and of homogeneous and inhomogeneous linewidths. It appears that the spectral shifts exhibit a weak $T$ dependence.[49] Accordingly, our general conclusions emerging from the analysis of $\delta\nu$ data hold in the range $T=10-40$ K, which constitutes "intelligent guesses" for the range of the temperatures of medium-sized $M\cdot A_n$ clusters.[7,8] The experimental spectra are rather congested to allow for the extraction of individual isomer-specific linewidths. Second, the supersonic expansion conditions, which allow for the formation of a "surface state" of perylene in perylene$\cdot Ar_n$ clusters should be further explored. As the relative abundance of structural isomers of $M\cdot A_n$ heteroclusters depends on the supersonic expansion conditions,[8,10] it is apparent that clustering in these systems is governed by kinetic rather than thermodynamic effects. Third, further investigation of one-sided surface states of perylene$\cdot Ar_n$ should be conducted preparing heteroclusters by crossing of a perylene beam with an $Ar_n$ beam. Fourth, studies of hole burning[22,37,49] should be conducted to sort out homogeneous isomer-specific line broadening.

## ACKNOWLEDGMENTS

A.H. is indebted to the Minerva Foundation for granting a postdoctoral fellowship. This research was supported by the German Israeli Binational James Franck program for laser–matter interaction.

[1] (a) U. Even, A. Amirav, S. Leutwyler, M. O. Ondrechen, Z. Berkovitch-Yellin, and J. Jortner, Faraday Discuss. Chem. Soc. **73**, 153 (1982); (b) S. Leutwyler and J. Jortner, J. Phys. Chem. **91**, 5558 (1987).
[2] (a) D. V. Brumbaugh, L. E. Kenny, and D. H. Levy, J. Chem. Phys. **78**, 3415 (1983); (b) T. A. Stephenson and S. A. Rice, J. Chem. Phys. **81**, 1083 (1984); (c) J. C. Alfano, S. J. Martinez, and D. H. Levy, Chem. Soc. Faraday Trans. **86**, 2503 (1990); (d) A. Heikal, L. Banares, D. H. Semmes, and A. H. Zewail, Chem. Phys. **156**, 231 (1991).
[3] S. Leutwyler and J. Bösiger, Chem. Rev. **90**, 489 (1990).
[4] J. Jortner, Z. Phys. D **24**, 247 (1992).
[5] A. Amirav, U. Even, and J. Jortner, Chem. Phys. Lett. **67**, 9 (1979).
[6] A. Amirav, U. Even, and J. Jortner, J. Chem. Phys. **75**, 2489 (1981).
[7] N. Ben-Horin, U. Even, and J. Jortner, J. Chem. Phys. **97**, 5988 (1992).
[8] N. Ben-Horin, U. Even, J. Jortner, and S. Leutwyler, J. Chem. Phys. **97**, 5296 (1992).
[9] J. Jortner, Ber. Bunsenges. Phys. Chem. **88**, 188 (1984).
[10] N. Ben-Horin, D. Bahatt, U. Even, and J. Jortner, J. Chem. Phys. **97**, 6011 (1992).
[11] S. Leutwyler and J. Bösiger, Z. Phys. Chem. NF **154**, 31 (1987).
[12] J. Bösiger and S. Leutwyler, Phys. Rev. Lett. **59**, 1895 (1987).
[13] J. Bösiger and S. Leutwyler, in *Large Finite Systems*, edited by J. Jortner and B. Pullman (Reidel, Dordrecht, 1987), pp. 153–164.
[14] S. Leutwyler and J. Bösiger, Faraday Discuss. Chem. Soc. **86**, 225 (1988).
[15] J. Bösiger, R. Knochenmuss, and S. Leutwyler, Phys. Rev. Lett. **62**, 3058 (1989).
[16] R. Knochenmuss and S. Leutwyler, J. Chem. Phys. **92**, 4686 (1990).
[17] (a) D. F. Kelley and E. R. Bernstein, J. Phys. Chem. **90**, 5186 (1986); (b) M. R. Nimlos, M. R. Young, and E. R. Bernstein, *ibid.* **91**, 5268 (1989).
[18] M. Schmidt, M. Mons, and J. Le Calvé, J. Phys. Chem. **96**, 2402 (1992).
[19] M. Schmidt, M. Mons, and J. Le Calvé, Chem. Phys. Lett. **177**, 371 (1991).
[20] M. Schmidt, M. Mons, J. Le Calvé, P. Millie, and C. Cossart-Magos, Chem. Phys. Lett. **183**, 69 (1991).
[21] M. Y. Hahn and R. L. Whetten, Phys. Rev. Lett. **61**, 1190 (1988).
[22] J. Bösiger, R. Bombach, and S. Leutwyler, J. Chem. Phys. **94**, 5098 (1991).

[23] A. Amirav and J. Jortner, Chem. Phys. **85**, 19 (1984).
[24] A. Amirav, M. Sonnenschein, and J. Jortner, Chem. Phys. **88**, 199 (1984).
[25] N. Ben-Horin, Ph.D. thesis, Tel-Aviv University, 1991, reported on pentacene·$Ar_n$ ($n=1-20$) data.
[26] T. Troxler and S. Leutwyler, Ber. Bunsenges. Phys. Chem. **96**, 1246 (1992).
[27] Structures of heteroclusters are labeled as follows: (i) $(n|m)$ marks $n$ atoms on one side and $m$ atoms on the other side of the aromatic molecule, both $n$ and $m$ being in the first layer. (ii) If further specification is required, $(n_2+n|m+m_2)$ labels $n,m$ atoms in the first layer on each side, and $n_2$, $m_2$ atoms in the second layer on each side of the aromatic molecule. When either $m_2=0$ or $n_2=0$, this number is omitted. (iii) $(n|m)+n_s$ and $(n_2+n|m+m_2)+n_s$ marks structure (i) or (ii) with additional $n_s$ atoms on the periphery of the aromatic molecule. When $n_s=0$ this number is omitted. (iv) $(n_3+n_2+n|m+m_2+m_3)$ marks a three layered structure with $n(m)$ atoms in the first layer and $n_j(m_j)$ atoms in layers $j=2,3$.
[28] S. Leutwyler, J. Chem. Phys. **81**, 5480 (1984).
[29] M. M. Doxtader, E. A. Mangle, A. K. Bhattacharya, S. M. Cohen, and M. R. Topp, Chem. Phys. **101**, 413 (1986).
[30] S. A. Schwartz and M. R. Topp, J. Phys. Chem. **88**, 5673 (1984).
[31] A. T. Amos, S. M. Cohen, J. C. Ketteley, T. F. Palmer, and J. P. Simons, in *Structure and Dynamics of Weak Molecular Complexes*, edited by A. Weber (Reidel, Dordrecht, 1987), p. 263.
[32] S. A. Wittmeyer, A. J. Kaziska, A. L. Motyka, and M. R. Topp, Chem. Phys. Lett. **154**, 1 (1989).
[33] A. J. Kaziska, S. A. Wittmeyer, A. L. Motyka, and M. R. Topp, Chem. Phys. Lett. **154**, 199 (1989).
[34] M. I. Shuchuka, A. L. Motykaard, and M. R. Topp, Chem. Phys. Lett. **164**, 87 (1989).
[35] S. A. Wittmeyer and M. R. Topp, Chem. Phys. Lett. **171**, 29 (1990).
[36] (a) A. J. Kayiska, S. A. Wittmeyer, and M. R. Topp, J. Phys. Chem. **95**, 3663 (1991); (b) A. J. Kayiska, M. I. Shuchuka, S. A. Wittmeyer, and M. R. Topp, *ibid.* **96**, 5017 (1991).
[37] A. J. Kayiska, M. I. Shuchuka, S. A. Wittmeyer, and M. R. Topp, J. Phys. Chem. **95**, 4627 (1991).
[38] C. L. Perkins, E. Perez, and K. M. Beck, Chem. Phys. Lett. **199**, 445 (1992).
[39] S. M. Ohline, P. W. Joireman, L. L. Connell, and P. M. Felker, Chem. Phys. Lett. **191**, 362 (1992).
[40] B. Fourmann, C. Jouvet, A. Tramer, J. M. Le Bars, and Ph. Millie, Chem. Phys. **92**, 25 (1985).
[41] A. Amirav (unpublished).
[42] F. Fillaux, Chem. Phys. Lett. **144**, 384 (1985).
[43] E. Shalev, N. Ben-Horin, U. Even, and J. Jortner, J. Chem. Phys. **95**, 3147 (1991).
[44] A. Heidenreich, D. Bahatt, N. Ben-Horin, U. Even, and J. Jortner, J. Chem. Phys. **100**, 6300 (1994), following paper.
[45] A. Heidenreich and J. Jortner, Z. Phys. D **26**, 377 (1993).
[46] L. Xinling, M. Y. Hahn, M. S. El-Shall, and R. B. Whetten, J. Phys. Chem. **95**, 8524 (1991).
[47] J. E. Adams and R. M. Stratt, J. Chem. Phys. **93**, 1358 (1990).
[48] A. Heidenreich and J. Jortner (to be published).
[49] B. Dick, E. Zinghar, and Y. Haas, Chem. Phys. Lett. **187**, 571 (1991).